Computers and Geotechnics 97 (2018) 27–41

Contents lists available at ScienceDirect

Computers and Geotechnics

journal homepage: www.elsevier.com/locate/compgeo

Research Paper

Dependence of ultimate bearing capacity and failure behavior of T-shaped deep cement mixing piles on enlarged cap shape and pile strength

Chana Phutthananon[a], Pornkasem Jongpradist[a,*], Phatharaphong Yensri[a], Pitthaya Jamsawang[b]

[a] Department of Civil Engineering, Faculty of Engineering, King Mongkut's University of Technology Thonburi, Thailand
[b] Department of Civil Engineering, King Mongkut's University of Technology North Bangkok, Thailand

ARTICLE INFO

Keywords:
Bearing capacity
Failure pattern
Shape factor
Finite element analysis
Small-scale physical model test
T-shaped deep cement mixing pile

ABSTRACT

A numerical investigation of the ultimate pile capacity (Q_{ult}) and failure behavior of T-shape deep cement mixing (TDM) piles is conducted under equivalent volume. Physical model tests are conducted to verify the numerical findings. The results reveal that both the shape of the enlarged pile cap and pile strength play key roles. Sensitivity analyses indicate that the effects of cap shape and pile strength on the complex load carrying behavior of TDM piles are attributable to changes in failure mode, which depend on the mobilized skin friction and bearing of both the cap and pile body.

1. Introduction

Soft ground improvement with deep cement mixing (DCM) piles is a soil stabilization technique that has been used to enhance the performance of on-ground and underground facilities, such as road embankments (e.g., [1–9]), drainage canals (e.g., [10,11]) and deep excavations (e.g., [12–14]). Since the first introduction of DCM piles in Sweden and Japan in the mid-1970s, this technique has been widely used in several countries where the soft ground layer is particularly thick [15]. The primary objectives of DCM piles include improving bearing capacity, minimizing lateral movement, reducing total and differential settlement, and increasing slope stability, as confirmed by many construction cases (e.g., [3,5,9]). Past experience also suggests that using DCM piles to improve soft ground areas reduces construction time and costs.

Generally, DCM piles are formed with the same cross-sectional area throughout their length (hereafter called a conventional DCM pile, see Fig. 1a) to transfer the applied load from the top part of the pile through the surrounding soil to the soil layer below the pile tip. Under an external load in the vertical direction, such as the foundation of a road or structure, the mobilized stress becomes largest at the pile head and then gradually decreases with depth. Thus, the highest compressive stress occurs at the top part of the pile, resulting in a failure pattern that is often dominated by pile head failure if the strength of the DCM pile is insufficient. This failure pattern has been confirmed by field test results in [16], in which more than half of tested conventional DCM piles failed due to pile head failure. When the pile head failure pattern is unfavorable, the cement content has been increased to enhance the strength of the conventional DCM pile. However, this is often an expensive strategy because the deeper pile does not require high strength. Moreover, many researchers (e.g., [17–19]) have revealed that the higher cement content does not economically improve the strength of cement-admixed clay. To solve the above-mentioned problem, new innovations of DCM pile techniques have been introduced, including stiffened and T-shaped DCM piles. A stiffened DCM (SDCM) pile is a composite DCM pile consisting of a DCM socket and stiffened core to reinforce the pile at shallow depths (or pile head) as shown in Fig. 1b. The T-shaped DCM (TDM) pile was first proposed in China [20,21]. The notable feature of TDM piles is that the diameter of the pile at shallow depth (surface pile diameter) is larger than that at greater depth (pile body diameter), resulting in a cross-sectional view of the TDM pile that resembles the letter "T" (see Fig. 1c).

A number of studies have investigated the efficacy of SDCM piles and their mechanical behavior, including full-scale field tests (e.g., [7,8]), numerical analyses (e.g., [7,8,22]) and physical model tests (e.g., [22]). The studies revealed that SDCM piles can resist higher loads than conventional DCM piles of the same size. Failure at the pile head under axial loading could also be mitigated. Based on these studies, the understanding of the impact of a stiffened core in associated with the strength of the DCM socket on ultimate pile capacity and failure behavior has been developed and continually updated. By contrast, studies on the efficacy and key influencing factors of the behavior of TDM piles are rather limited, probably because this innovation is still relatively new. Based on the results from full-scale field tests and small-

* Corresponding author at: Civil Engineering Department, Faculty of Engineering, King Mongkot's University of Technology Thonburi, 126 Pracha Uthit, Bang Mod, Thung Khru, Bangkok 10140, Thailand.
E-mail address: Pornkasem.jon@kmutt.ac.th (P. Jongpradist).

https://doi.org/10.1016/j.compgeo.2017.12.013
Received 15 November 2017; Received in revised form 15 December 2017; Accepted 26 December 2017

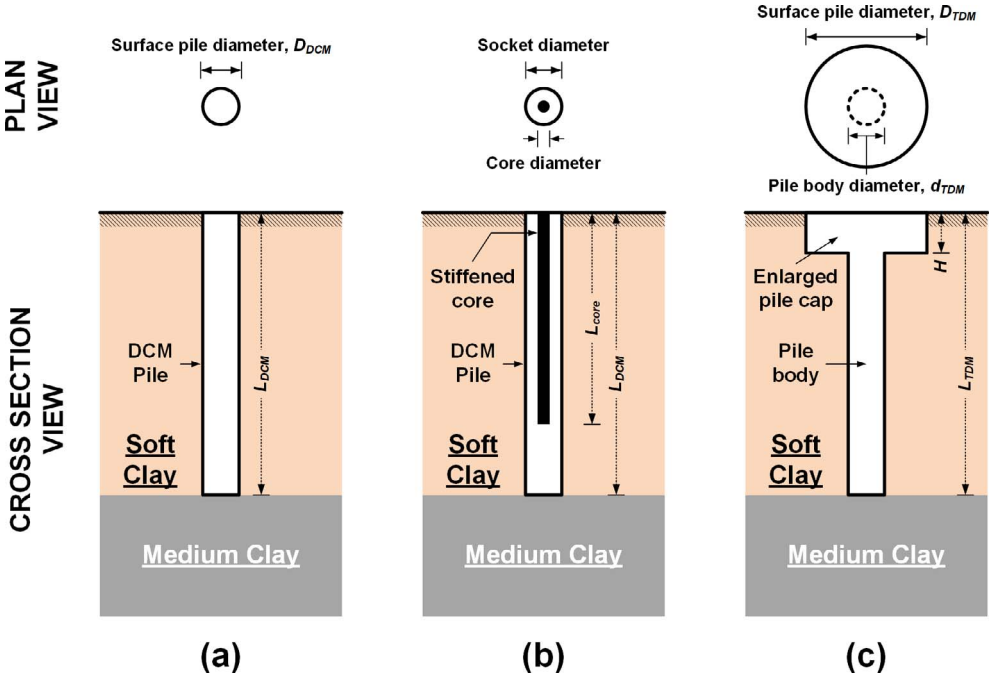

Fig. 1. Schematic of DCM piles: (a) conventional DCM pile; (b) SDCM pile and (c) TDM pile.

scale physical model tests [23,24], enlarging the pile cap (from a DCM pile to a TDM pile), the bearing capacity can be increased, and settlement can be reduced. Physical model tests also revealed that, for a TDM pile, failure occurs at the pile body immediately below the enlarged pile cap. This failure mode implies an association with the bearing capacity of the TDM pile. Under the embankment loading condition as the foundation in physical model tests [25], the enlarged pile cap of a TDM pile provided a higher pile efficacy (defined as the ratio of load carrying at the pile to the entire applied load on the embankment) than a conventional DCM pile. Moreover, TDM piles are more effective in reducing differential settlement between the surrounding soil and the pile. All of these studies indicate the superior performance of TDM piles over conventional DCM piles with the same pile body and strength. However, each of these previous studies focused on an increase of either the diameter or length of enlarged pile cap without consideration on the pile volume. Enlarging the pile cap increases construction costs due to the additional volume of improvement by cement. Consequently, the evaluation of the performance and effectiveness of a TDM pile should be compared with those of a conventional DCM pile on an equal volume basis. Based on the mechanism established in previous studies, it is possible to reduce the size of the pile body while introducing an enlarged pile cap. Moreover, it is assumed that the size of the enlarged pile cap will have an effect on the complex load transfer mechanism of the TDM pile, which, in turn, affects the bearing capacity and failure behavior.

The goal of this work is to study the effect of the size of the enlarged pile cap and pile strength on the behavior of TDM piles in terms of ultimate bearing capacity and failure pattern under controlled pile volume. Numerical analyses of the selected cases of piles under axial loading are preliminarily performed. The total volumes of piles with various shapes and strengths are controlled. A parameter “shape factor” is introduced based on the condition of the control pile volume to assist the interpretation of the results. Small-scale physical model tests under conditions of shape factor equivalent to those in the preliminary investigation are conducted to validate the findings. Finally, a numerical sensitivity study of TDM piles is performed by varying the dimensions of the enlarged pile cap and the strength of the pile with a single value of pile volume to observe changes in ultimate bearing capacity and failure pattern. The complex interaction between the shape of the enlarged pile cap and the strength of the pile is revealed and discussed. Note that deformation behavior is not discussed in the present work.

2. Case history and numerical modelling

This paper offers a series of two-Dimensional (2D) finite element analyses to investigate the ultimate bearing capacity and failure pattern of DCM and TDM piles under axial compression load. First, the numerical method and parameters used were validated by comparing the simulated results with the field pile load test data [26] in term of load-settlement curve at the head of DCM pile. Then, they were adopted to analyze the ultimate bearing capacity and failure pattern of DCM and TDM piles in the sections of preliminary investigation and sensitivity study.

2.1. Case history

Over the past 10 years, TDM piles have been proposed and constructed to support highway embankments in China [20,21]. Because this technology is relatively new, its application and study have not yet spread to other countries. As a result, information on field TDM pile load tests is scarce. In this study, a case study of a previous full scale axial load test of a conventional DCM pile [26] was chosen. The test site was located at the campus of Asian Institute of Technology (AIT) in the Lower Central Plain of Thailand. The field data were used to verify the analysis method of the study. The subsoil profile and some engineering properties of the test site are summarized in Fig. 2. The soil profile at this site comprises a 1.5-m-thick weathered crust underlain by soft clay with a thickness of approximately 5.0–6.5 m. The undrained shear strength obtained from field vane tests of the soft clay was 16–17 kPa. A medium clay with an undrained shear strength greater than 30 kPa was found below the soft clay. The groundwater level was approximately 1.5 m below the ground surface. The conventional DCM pile was constructed in situ by the wet jet mixing method with a cement content of 150 kg/m^3 of soil and a jet pressure of 22 MPa. The length and surface pile diameter of the tested DCM pile were 7.0 m and 0.6 m, respectively. The average value of unconfined compressive strength was approximately 900 kPa. The top of the DCM pile was situated 1.0 m below the ground surface.

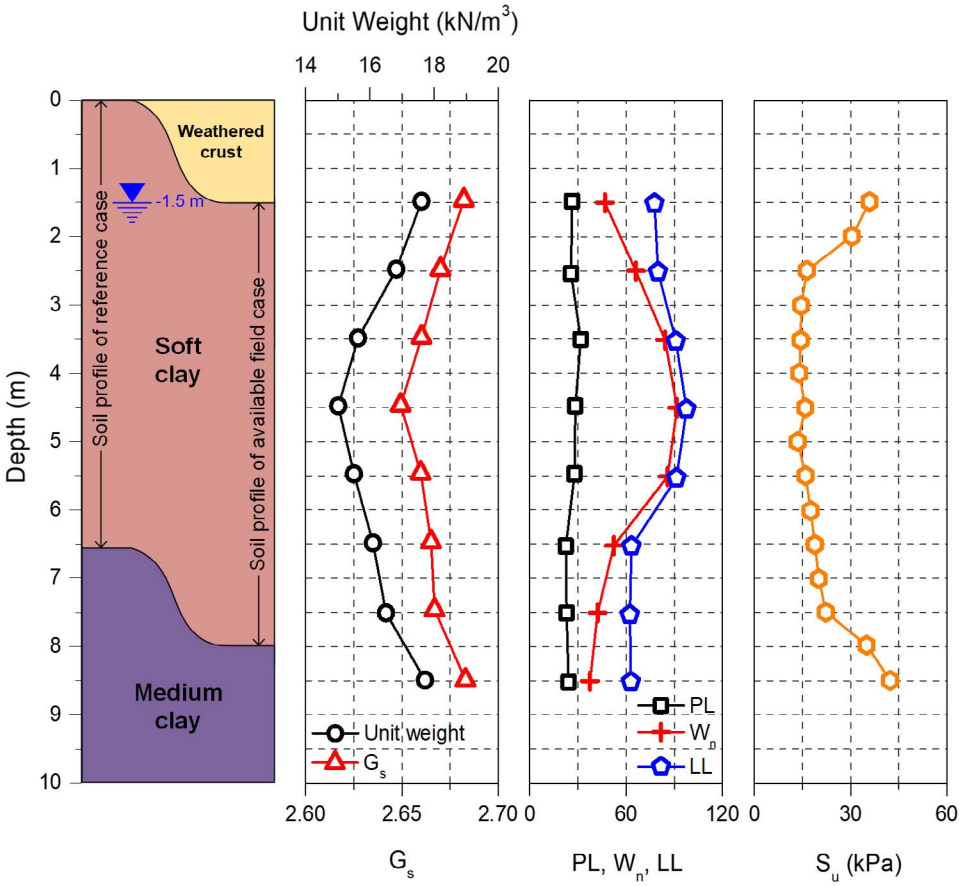

Fig. 2. Subsoil profile of case history and reference case.

2.2. Numerical modelling

2.2.1. Finite element mesh and boundary conditions

A series of 2D finite element (FE) simulations were performed to investigate the mechanical behavior of the conventional DCM and TDM piles under axial compression loading, including the ultimate bearing capacity (Q_{ult}) and failure pattern. The continuum FE software PLAXIS 2D was used. Fig. 3 shows an example of the FE mesh used in the axisymmetric analysis, which consisted of a 25.0-m-deep and 10.0-m-wide domain. The boundary condition for the FE mesh was that both side boundaries were prevented from moving in the horizontal direction, whereas the bottom boundary was prevented from moving in both the horizontal and vertical directions. These conditions were used in all pile load test simulations. The conventional DCM pile, TDM pile and soils were modelled using fifteen-node hybrid triangle elements. For the initial distribution of horizontal and vertical stresses, the soil unit weight and the coefficient of earth pressure were used to calculate the initial soil stress state. The initial pore water pressure was assumed to be hydrostatic. The simulation was divided into five main steps: (i) generation of the stress field and hydrostatic pore water pressure, (ii) excavation of a 1-m-deep pit from the ground surface, (iii) installation of conventional DCM or TDM piles, (iv) installation of a rigid steel plate at the pile top with the same diameter to accommodate the distribution of stresses evenly, and (v) applying an axial load on top of pile the in 10-kN increments until failure occurred. The Q_{ult} values of the DCM and TDM piles were determined from the load-settlement curve using the classic slope tangent method in double logarithmic scale following De Beer [27]. The settlement of the pile was measured at the center of the pile head surface. The weathered crust layer was replaced by a soft clay layer in all preliminary and sensitivity analysis cases to avoid complex interactions between the crust and the enlarged pile cap. Due to the limited depth of the testing box in the physical model tests (see details in section 4), the thickness of the soft clay layer was also decreased from 8.0 m in the available field case to 6.6 m in the numerical investigation to maintain a scaling factor of 13 for the purposes of comparison. Consequently, the length of the piles in the preliminary investigation (section 3) and sensitivity analyses (section 5) was 5.6 m.

2.2.2. Constitutive model and model parameters

In this study, a Mohr-Coulomb (MC) model and a Hardening Soil (HS) model [28] coded in PLAXIS program were applied to the FE analysis. The effective stress analysis under undrained behavior was conducted to simulate the quick pile load tests in the field. The undrained function of material type, namely Undrained, was specified in PLAXIS program in which the effective stress parameters for both soil modulus and shear strength were assigned.

The behavior of the DCM and TDM piles was modelled by the MC model, whereas the HS model was applied to model the behavior of the soft clay, medium clay and stiff clay. For the rigid steel plate, a linear elastic (LE) model was used. The properties of the materials in the numerical analyses are listed in Table 1. The values of the parameters considered in this study are all effective values. For the soil parameters (HS model) of Bangkok subsoil, the parameter sets were adopted from the work of Rukdeechuai et al. [29]. The HS model parameters were mainly calibrated from the triaxial and oedometer testing results of soil samples taken from the Asian Institute of Technology (AIT) together with the field measurement conducted by Prust et al. [30]. These parameter sets have been used to analyze various geotechnical works in Bangkok subsoil (e.g., [29,31,32]). Note that the elastic moduli of the DCM and TDM piles were determined from the simple correlation $E_{SCP} = 113q_u$, where E_{SCP} is the modulus of elasticity in terms of secant ($50\% of q_u$) and q_u is the unconfined compressive strength of the soil-cement pile. This correlation falls within the range of $20q_u$–$360q_u$ for cement-treated clays reported by Voottipruex et al. [8] and Jamsawang

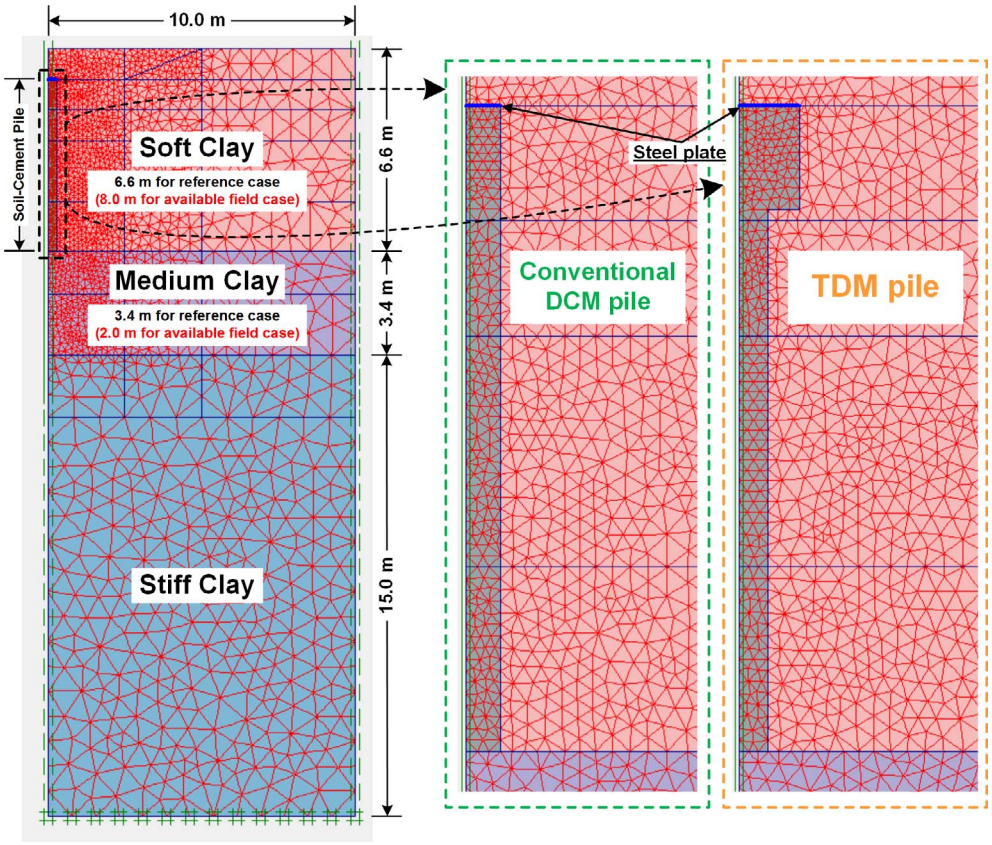

Fig. 3. Geometry, finite element mesh and boundary conditions of the considered problem.

et al. [33] and closes to those used in several previous publications (e.g., [3,34,35]). After converting to effective parameter, the correlation becomes $E'_{SCP} = 100q_u$, which corresponds to previous work of Wonglert and Jongpradist [22].

2.2.3. Verification with field measurement

To verify the analysis method used in this work, the analysis results were compared with the measurement data for a full-scale conventional DCM pile load test [26]. The axial load-settlement curves for the computed and measured results are compared in Fig. 4. The load-settlement curve of the conventional DCM pile from the FE model matches well with the field test results. Therefore, the analysis method and sets of parameters used were considered appropriate for further numerical investigation.

3. Preliminary investigation

In the preliminary investigation, 2D FE axis-symmetry analysis was conducted to examine the impact of key influencing parameters on the Q_{ult} and failure behavior of the conventional DCM and TDM piles. The

Table 1
Materials models, and parameters used in this study.

	Unit	Weathered crust	Soft clay	Medium clay	Stiff clay	DCM pile[a]	Rigid steel plate
Model		MCM	HSM	HSM	HSM	MCM	LE
Material behavior		D	U	U	U	U	Elastic modulus = 10^{12} kPa and Poisson's ratio = 0
Elastic modulus, E'	kPa	5000	–	–	–	90,000	
Secant stiffness, E_{50}^{ref}	kPa	–	5000	20,000	60,000	–	
Tangential stiffness, E_{oed}^{ref}	kPa	–	5000	20,000	60,000	–	
Unloading and reloading stiffness, E_{ur}^{ref}	kPa	–	15,000	100,000	180,000	–	
Poisson's ratio for unloading–reloading, ν_{ur}	kPa	0.25 (=ν')	0.20	0.20	0.20	0.33 (=ν')	
Power of the stress level dependency of the stiffness, m	(–)	–	1	1	1	–	
Coefficient of earth pressure at rest (NC state), K_0^{NC}	(–)	0.600	0.625	0.625	0.625	0.577	
Unit weight, γ	(kN/m^3)	17	15	15	18	15	
Effective cohesion, c'	(kPa)	8	6	10	18	423	
Effective friction angle, ϕ'	(degree)	22	22	22	22	25	
Angle of dilatancy, ψ	(–)	0	0	0	0	0	
Failure ratio, R_f	(–)	–	0.9	0.9	0.9	–	
Over consolidation ratio, OCR	(–)	–	1.1	2.0	2.5	–	
Reference stress, p^{ref}	(kPa)	–	100	65	95	–	

[a] Case history, Material behavior; D = drained, U = undrained.

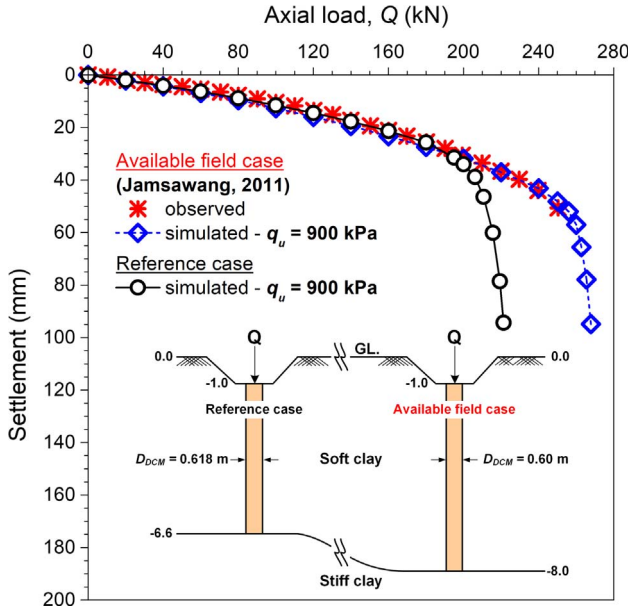

Fig. 4. Comparisons of observed (available field case) and computed (available field and reference cases) axial compression load-settlement curves of conventional DCM piles.

key parameters studied were the surface pile diameter of the conventional DCM piles (D_{DCM}) and TDM piles (D_{TDM}) and the strength (q_u) of the piles. The pile lengths, L_{DCM} and L_{TDM}, and pile body diameter (d_{TDM}) were fixed at 5.6 m and 0.5 m, respectively, throughout the study. The thickness of the enlarged pile cap (H) was varied following D_{TDM} under the condition of pile volume control.

3.1. Effect of surface diameter and strength of the conventional DCM pile on the load-settlement curve compared to the reference case

To provide information for comparison with the TDM piles (in the next subsection), analyses with various values of D_{DCM} and q_u were performed. The three values of D_{DCM} were 0.50 m, 0.618 m (reference case), and 0.70 m. The load-settlement curves are shown in Fig. 5. The results imply that Q_{ult} increases as D_{DCM} increases at the same pile

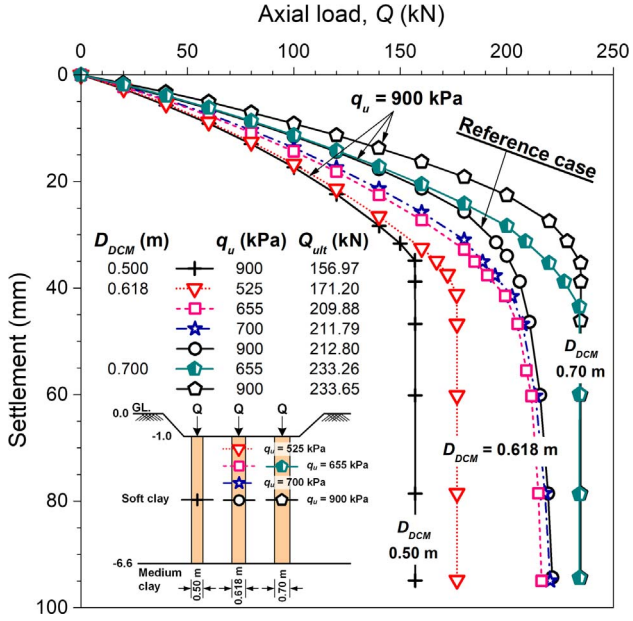

Fig. 5. Effects of pile diameter and strength on the load-settlement curves of conventional DCM piles.

strength, as expected. Moreover, at the same load level, an increase in D_{DCM} significantly leads to decreasing settlement. This effect is caused by the side resistance along the shaft of the pile and tip resistance from the soil below the pile tip. The pile with a higher value of D_{DCM} possesses a larger area of the pile shaft and cross-sectional area of the pile tip, with higher ultimate bearing capacities. To investigate the failure patterns of these piles, the occurrence of plastic points (Mohr-Coulomb points, MCPs in the PLAXIS program) is observed from the simulation results at the applied load of Q_{ult}, as depicted in Fig. 6. MCPs of the DCM piles (D_{DCM} = 0.50,0.618, and 0.70m with q_u of 900 kPa) were found only in the surrounding soil, indicating a soil failure pattern (see Fig. 6a, e and g). These results clearly indicate that the surface pile diameter of the conventional DCM pile plays an important role in Q_{ult} and settlement.

The results of further investigations of the effect of q_u on Q_{ult} are presented in Fig. 5. Piles with D_{DCM} of 0.618 m and varying q_u, including 900 kPa (reference case), 700 kPa, 655 kPa and 525 kPa, were chosen for investigation. The modulus of elasticity was also adjusted to correspond to the correlation described in Section 2.2.2. The Q_{ult} of the conventional DCM pile increased considerably (171.20–209.88 kN) as q_u increased from 525 kPa to 655 kPa. For the case of q_u = 525 kPa, MCPs occurred at the top part of the pile and propagated to the surrounding soil on the periphery of the pile until a depth of 2.5 m below ground surface was reached (see Fig. 6b). Thereafter, the failure pattern was dominated by pile head failure. As q_u increased to 655 kPa, MCPs also propagated in the surrounding soil throughout the pile length (see Fig. 6c), eventually leading to pile head failure (many MCPs at the top part) together with a soil failure pattern. The number of MCPs at the top part of the pile for the case of q_u = 655 kPa was less than for a pile strength of 525 kPa. As q_u increased from 655 kPa to 700 kPa, Q_{ult} slightly increased to approximately 1.91 kN with the same failure pattern as in the case of q_u = 700 kPa. A larger number of MCPs mostly appeared at the soil below the pile tip (see Fig. 6d). Up to a q_u of 900 kPa, Q_{ult} exhibited insignificant development. Additionally, the failure pattern changed to perfect soil failure, with no MCPs occurring in the pile (see Fig. 6e). These results indicate that the q_u of 700 kPa is the optimum value of pile strength to produce the highest Q_{ult}. However, for the same load level, increasing the q_u over the optimum value reduces pile settlement (see Fig. 5). Therefore, it can be concluded that, for the case of q_u less than the optimum value, Q_{ult} is primarily dependent on q_u. By contrast, when q_u is larger than optimum value, Q_{ult} does not significantly develop. Nevertheless, using q_u higher than the optimum value can reduce pile settlement. Moreover, q_u is also a major parameter influencing the failure pattern of the conventional DCM pile. This conclusion was confirmed by the results for the conventional DCM pile, with D_{DCM} = 0.70 m at q_u of 655 and 900 kPa (see Fig. 5). In both piles, the failure pattern was governed by soil failure (see Fig. 6f and g). Moreover, the optimum value of pile strength is related to the surface diameter of the DCM pile and the soil condition.

3.2. Effect of an enlarged pile cap dimension and strength of the TDM pile on the load-settlement curve compared to the conventional DCM pile under controlled volume

The effects of the transformation to a TDM pile and of the enlarged pile cap dimension on the load-settlement curves are numerically investigated in this section. TDM piles with a volume equivalent to that of the conventional DCM pile with a diameter of 0.618 m and a length of 5.6 m was considered. The pile body diameter of 0.5 m was fixed while the enlarged cap size (surface diameter, D_{TDM} and thickness, H) was varied within the same pile volume. Two values of q_u of the pile (525 and 655 kPa) are considered. D_{TDM} values of 0.73, 0.988, 1.17 and 1.32 m with corresponding H values of 2.62, 1.04, 0.65 and 0.50 m, respectively, are considered in the analyses. The simulated load-settlement curves are illustrated in Fig. 7. The values of calculated Q_{ult} are also reported in the figure. For piles with q_u of 525 kPa (Fig. 7a), the

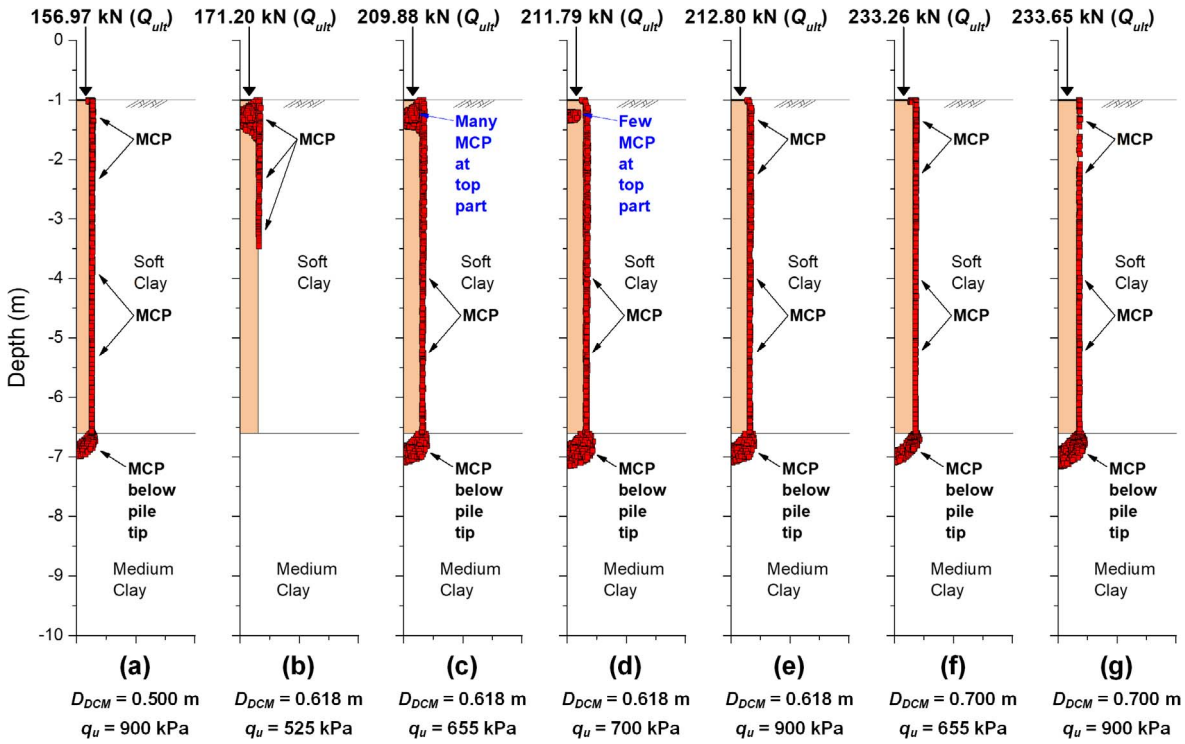

Fig. 6. Failure patterns of conventional DCM piles with various pile diameters and strengths.

results clearly indicate that the change in the pile shape from conventional DCM (D_{DCM} = 0.618 m) to TDM (D_{TDM} up to 1.32 m) leads to an increase in Q_{ult} and reduction of pile settlement at the same load level. Note that Q_{ult} decreases with increasing D_{TDM} from 0.73 to 0.988 m before increasing again when D_{TDM} is 1.17 m. However, Q_{ult} is still greater for D_{TDM} = 0.988 m than for D_{DCM} = 0.618 m.

A dissimilar result was observed for the piles with a q_u of 655 kPa, as shown in Fig. 7b. The values of Q_{ult} slightly decreased as the pile shape changed from conventional DCM to TDM with D_{TDM} = 0.730 and 0.988 m. As D_{TDM} increased to 1.17 m, Q_{ult} increased. Additional insights can be obtained by comparing the results for a pair of selected cases, as shown in Fig. 7c. Q_{ult} of the case for the TDM pile with D_{TDM} of 1.17 m and q_u of 655 kPa is nearly identical to that for the DCM pile of 0.618 m (same pile volume) and q_u of 900 kPa (upper subfigure). These results indicate the potential to reduce the pile strength (i.e., the cement content) while enlarging the pile cap to achieve the same pile capacity. In the lower subfigure, at the same pile strength (655 kPa in this case), Q_{ult} of the TDM pile with D_{TDM} of 1.32 m is almost identical to that of the 0.700-m-diameter DCM pile (larger pile volume). This result indicates the potential to reduce the pile volume while enlarging the pile cap to achieve the same pile capacity. These results confirm the benefits of using TDM piles to reduce construction costs.

The above observations imply that the change from a conventional DCM pile to a TDM pile can offer benefits by reducing either the pile volume or strength for a target pile capacity. However, the effectiveness of the change from a conventional DCM pile to a TDM pile depends on the design of an appropriate shape. A better understanding of the load carrying behavior of TDM piles is necessary. Moreover, both the shape of the pile cap and q_u play important roles in this load carrying behavior. To accommodate the representation of the results regarding the enlargement of pile cap shape, an empirical "shape factor (α_s)" taking the geometry of the TDM pile into account, is hereafter used. Based on the fact that, with continually enlarging the pile cap, the surface diameter and skin area of the TDM piles become larger and smaller, respectively, compared to those of the DCM pile at the same volume. The ratio of bearing area of TDM pile to DCM pile over the ratio of shaft area of TDM pile to DCM pile as shown in Eq. (1) is thus appropriate.

$$\alpha_s = \frac{D_{TDM}^2/D_{DCM}^2}{[(D_{TDM}-d_{TDM})H + d_{TDM}L_{TDM}]/D_{DCM}L_{DCM}} \quad (1)$$

Under a controlled volume and constant pile body diameter, a larger value of α_s indicates a larger but thinner pile cap. The value of α_s for a conventional DCM pile is equal to 1.0. Note that the α_s in the present form is for a controlled volume and constant pile body diameter, further development may be necessary if it will be applied for other conditions. The Q_{ult} values from Fig. 7a and b were plotted against α_s, as shown in Fig. 8, confirming the significant effects of both the shape of the enlarged pile cap and q_u on pile capacity. The transformation to a TDM pile with a small (but thick) cap can either increase or decrease Q_{ult} compared to the originally considered DCM depending on the pile strength.

The failure patterns of the piles were further investigated to obtain insights on the load carrying behavior in association with the failure behavior. The developed MCPs at the applied load of Q_{ult} of piles with q_u of 525 and 655 kPa are illustrated in Fig. 9a–d and e–h, respectively. At q_u of 525 kPa, MCPs occur in the soil surrounding the pile for the entire length (see Fig. 9a), indicating a change in the failure pattern from pile head failure for the DCM pile (see Fig. 6b) to soil failure for the TDM pile with small cap diameter. For the other three TDM piles with larger but thinner pile caps, MCPs occurred at the pile body immediately beneath the enlarged pile cap, indicating "pile body failure" (see Fig. 9b–d). This failure pattern corresponds to that observed in field tests by Yi et al. [24]. As q_u increases to 655 kPa, the conventional DCM pile failed due to pile head failure simultaneous with soil failure (see Fig. 6c). Transformation to TDM piles resulted in a mode of soil failure in which MCPs occurred in the surrounding soil (see Fig. 9e–h). Moreover, the results for these TDM piles indicated that only a few MCPs occurred at the pile body, immediately below the enlarged pile cap. These results indicate that the failure pattern of conventional DCM piles and TDM piles depends greatly on cap shape and pile strength.

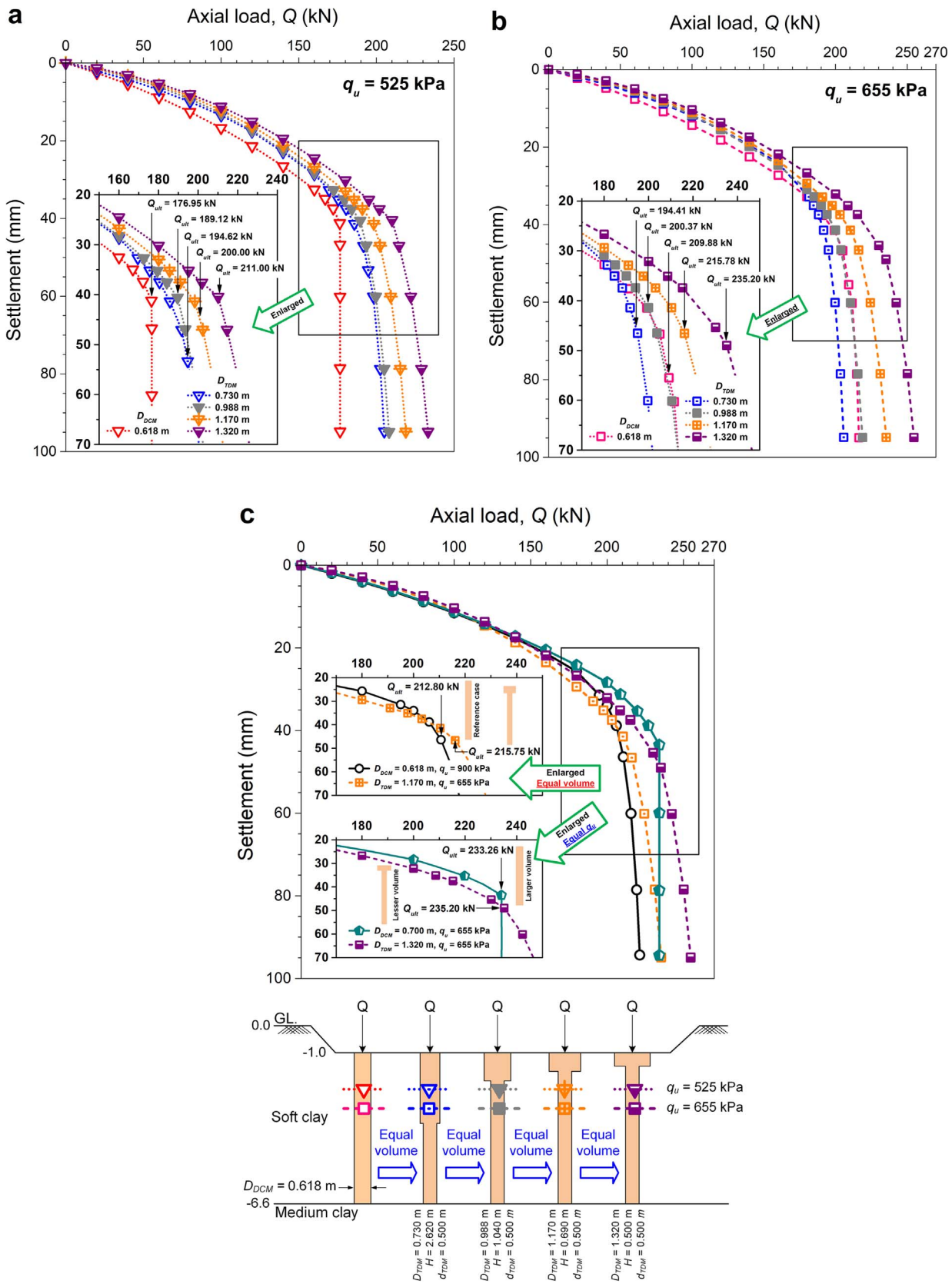

Fig. 7. Effect of an enlarged pile cap dimension of TDM piles with various strengths: (a) q_u = 525 kPa and (b) q_u = 655 kPa. (c) Comparisons of the effectiveness of conventional DCM and TDM piles with equivalent volume and strength.

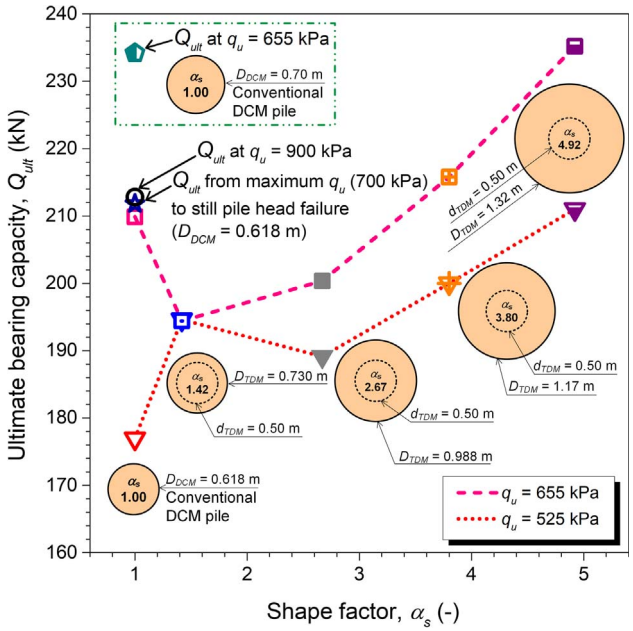

Fig. 8. Changes in ultimate bearing capacity due to the transformation of a DCM pile to a TDM pile under the controlled volume condition.

4. Physical model test

To verify the results of the preliminary investigation analysis with respect to changing Q_{ult} under different α_s, a series of small-scale physical model tests were conducted under equivalent pile volume. Three values of α_s from the preliminary investigation (1.00, 2.67 and 3.80) were selected to construct the model piles in the laboratory. These model piles were tested under vertical loading. A scaling factor of 13 was chosen for this small-scale physical model to reduce the dimensions of the prototype piles. The tests included a ground model and four models of soil-cement piles, as shown in Fig. 10. Two conventional DCM piles with different sizes and volumes and two TDM piles with different pile cap sizes but the same volume were prepared under the same target pile strength. The models of the conventional DCM piles had D_{DCM} = 38 mm and L_{DCM} of 430 mm for the P1 pile (equivalent to the 0.5-m @5.6-m-long DCM pile of the prototype) and D_{DCM} = 47 mm for the P2 pile (equivalent to the 0.6-m @5.6-m-long DCM pile of the prototype). The models of the TDM piles (P3, α_s = 2.72; P4, α_s = 3.88 piles) had the same volume and length as the P2 pile. The dimensions of the enlarged pile cap for the P3 pile were as follows: surface pile diameter of 76 mm; thickness of the enlarged cap of 80 mm; pile body diameter of 38 mm. A larger surface pile diameter of 90 mm and a thinner enlarged cap of 53 mm were used for the P4 pile. The ground model in this study included consolidated remolded soft clay and artificial medium clay. The soft clay was prepared by consolidating remolded soft Bangkok clay, which was mixed with water to achieve a total remolded water content of 100%, to attain the target water content of 70%. The artificial medium clay was prepared from a mixture of the remolded clay slurry and Ordinary Portland Cement type I at a cement content (defined as the ratio of the weight of cement to the weight of dry soil) of 5%. Before installation of the ground model, the inner sides of the rigid test box (1000 × 400 × 1800 mm, deep × wide × long, see Fig. 10) were smeared with grease to minimize the effect of friction. Then, the box was filled with the mixture of medium clay and cured for 7 days. Subsequently, the remolded clay slurry was poured on the artificial medium clay layer and consolidated with an applied surcharge load (5.2 kN/m^2) for 60 days. After completion of the consolidation process, the models of the soil-cement piles were constructed by using PVC tubes as the pile casing to create a hole for the cement-admixed clay paste. The remolded clay slurry was mixed

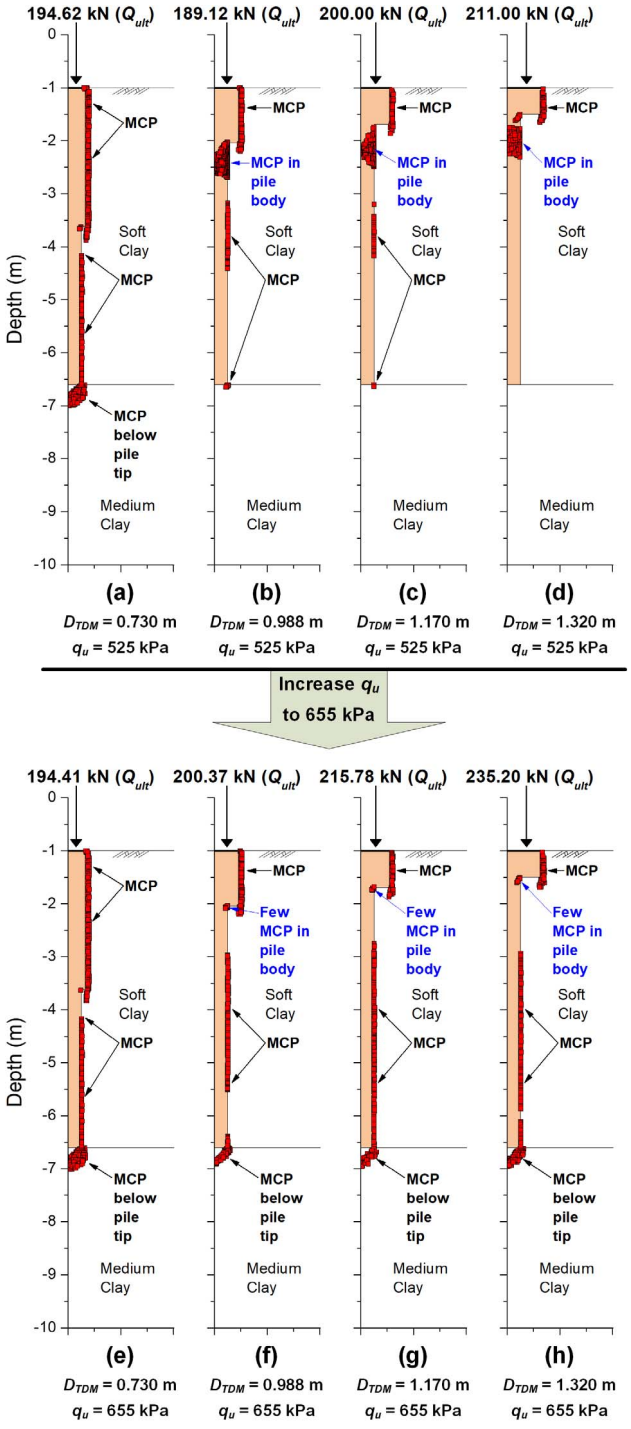

Fig. 9. Failure patterns of conventional DCM and TDM piles under controlled volume with strengths of 525 kPa and 655 kPa.

with a 35% content of Ordinary Portland Cement type I. The target unconfined compressive strength (q_u) of all of the soil-cement piles was 760 kPa. To ensure the target q_u of the soil-cement piles, on-site samples were collected and tested to confirm the strength with a curing time of 28 days. The method for the pile load test was the quick loading test in accordance with "ASTM-D1143". All tests were performed at an incremental axial compression load of 15 N (under the stress control condition) in each loading stage (every 5 min) with an axial penetration load rate of 5 N/min until failure. A pneumatic control system and a computer were used to regulate the pressure in four air cylinders, followed by transfer to a piston rod to press the modelled footing on the

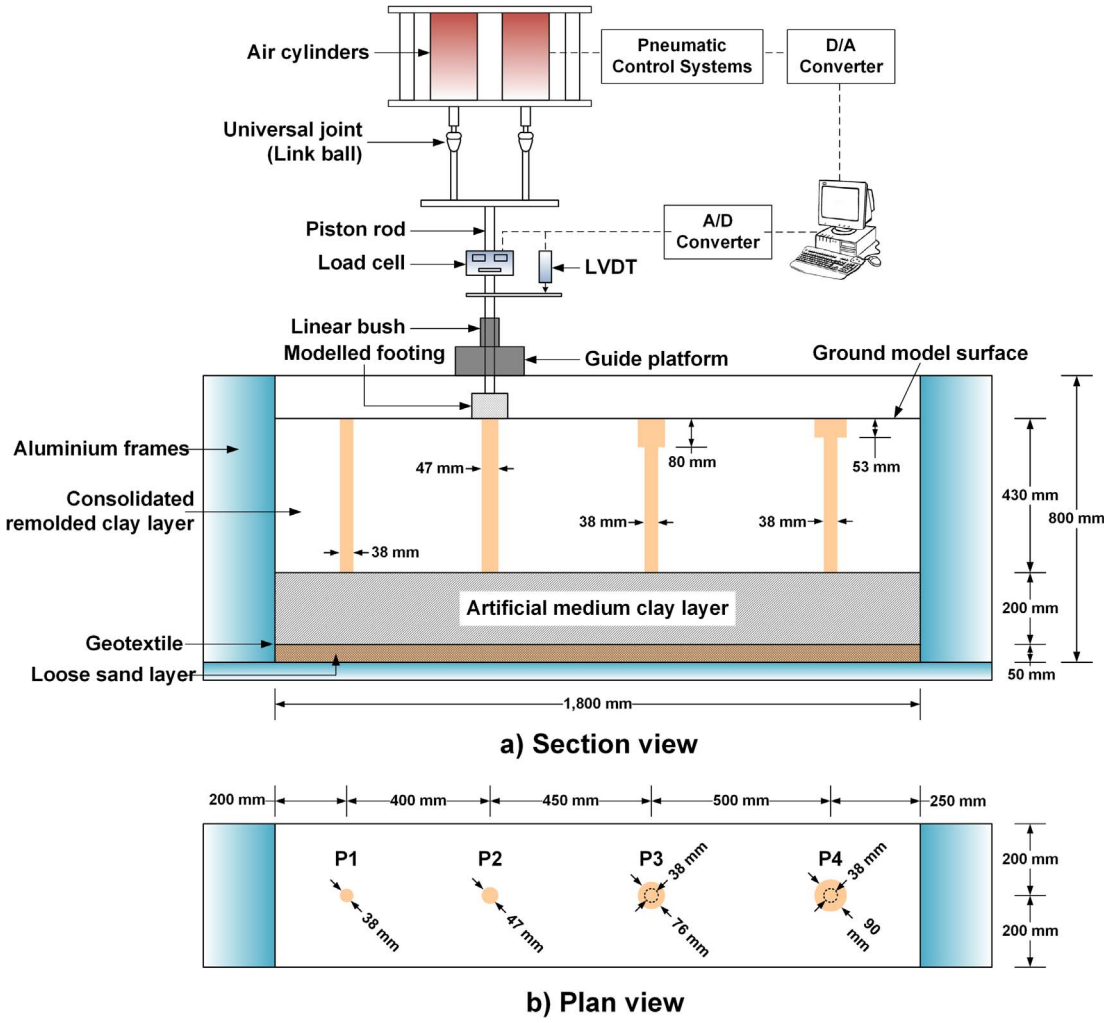

Fig. 10. Soil-cement piles and equipment configuration of the small-scale physical model tests.

pile surface. The value of the axial load was measured and recorded automatically by a load cell and the computer together with a data logger system. A Linear Variable Differential Transformer (LVDT) was used to measure the settlement of the soil-cement pile situated at the piston rod. The details of the equipment configuration are shown in Fig. 10.

After the loading test, the soil around the piles was meticulously excavated to observe the failure of the piles, as illustrated in Fig. 11. The head of the P2 pile (conventional DCM pile) was completely broken (see Fig. 11a). For the P3 pile (TDM pile), small cracks were observed approximately 60 mm below the enlarged pile cap (see Fig. 11b). A crack was observed at the pile body immediately below the enlarged pile cap for the P4 pile (TDM pile) (see Fig. 11c).

The load-settlement curves of the conventional DCM (P1-P2) and TDM (P3-P4) model piles from the laboratory loading tests are presented in Fig. 12. Q_{ult} of the P1 and P2 piles was 0.225 kN and 0.675 kN,

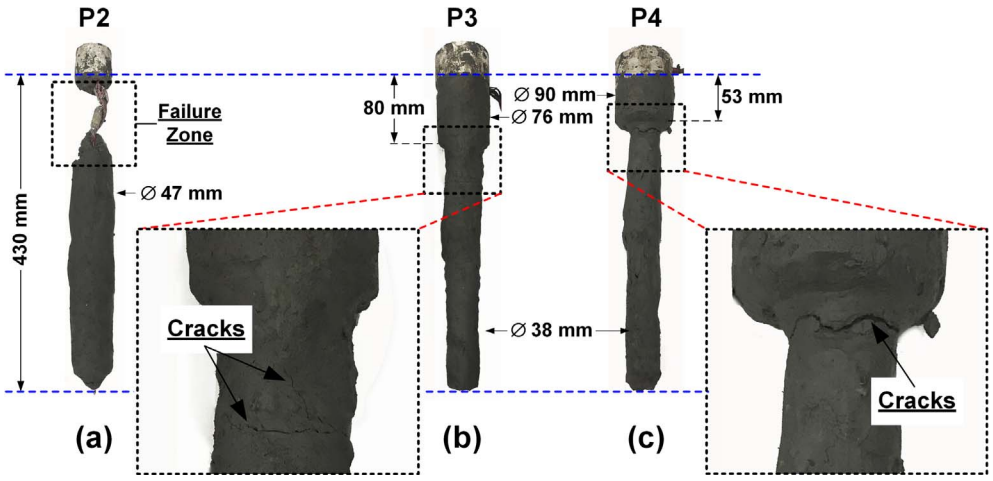

Fig. 11. Photographs showing the failure patterns of conventional DCM and TDM piles after testing.

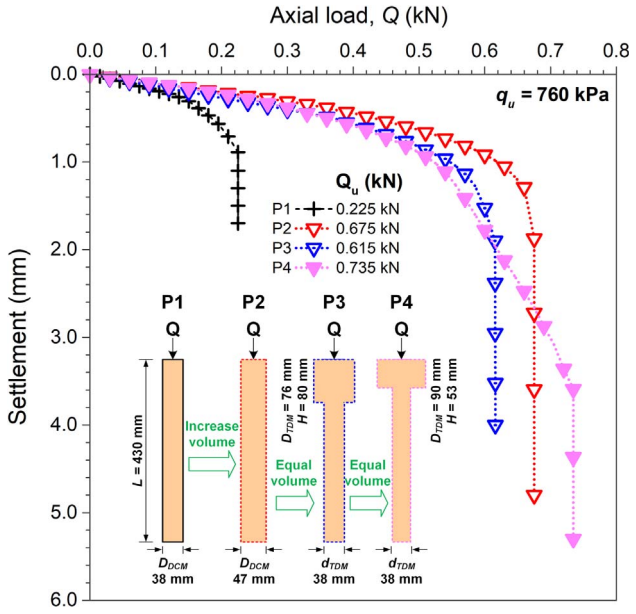

Fig. 12. Load-settlement curves of conventional DCM and TDM piles from the physical model tests.

respectively. Q_{ult} of the P2 pile was 3 times higher than that of the P1 pile because the P2 pile had a larger surface pile diameter, resulting in larger tip and side resistances. Additionally, the curve of the P2 pile shows smaller settlements than that of the P1 pile at the same load level. These observations are consistent with the results of the preliminary investigation in section 3.1. For the DCM and TDM piles with the same pile volume, the curves of the P2, P3 and P4 piles were nearly identical when the axial load was less than 0.3 kN. Once the axial load exceeded 0.3 kN, the curve of the P4 TDM pile indicated larger settlements than those of the other two piles. However, the P4 pile can sustain a larger maximum load, and the P3 TDM pile exhibited a smaller pile capacity than the P2 DCM pile. The results of the small-scale physical model tests are in good qualitative conformity with the results of the preliminary investigation in section 3.2. Enlarging the pile cap does not always guarantee an increase in the pile ultimate capacity. Q_{ult} is strongly influenced by the shape of the enlarged pile cap. Thus, the FE model provides confidence for the further investigations of the behavior of TDM piles in the next section. Not all properties can be maintained between the physical model tests and the numerical investigation in the previous section. However, these differences are unlikely to affect the qualitative conclusions obtained from the physical model tests and the numerical analyses.

5. Sensitivity study

To comprehensively investigate the effect of an enlarged pile cap shape of a TDM pile and pile strength on Q_{ult} and the failure pattern, numerical sensitivity analyses were performed. The pile volume in all cases was equal to the conventional DCM pile, with D_{DCM} = 0.618 m and L_{DCM} = 5.6 m. The pile with a q_u of 700 kPa (optimum value) was set as the baseline case to compare the effectiveness for Q_{ult}. The preliminary investigation indicated that the behavior of TDM piles is strongly influenced by the interaction between (1) the shape of the enlarged pile cap, which can be represented by the shape factor (α_s), and (2) the strength of the soil–cement pile (q_u). To analyze the influence of the shape of the cap, thirteen values (cases No. 2–14) of D_{TDM} and H were considered in ranges of 0.68–1.50 m and 0.37–3.49 m, respectively. d and L_{TDM} were maintained constant of 0.5 m and 5.6 m, respectively. Fig. 13 shows a schematic of the shapes of the DCM and TDM piles in this parametric study. q_u ranged from 320 to 700 kPa. All cases investigated are summarized in Table 2. The strength ratio (α_p) was used to denote the strength of the soil–cement pile in each case compared to the baseline case or optimum pile strength (700 kPa in this study) which provides the highest ultimate bearing capacity (depends on size of DCM pile) as described in ection 3.1. The α_p can be expressed in Eq. (2).

$$\alpha_p = \frac{q_u \text{ in each case}}{q_u \text{ of baseline case}} \tag{2}$$

(1) Failure patterns

The objective of a DCM pile is to transfer the applied load from the shallow depth to deeper strata that are stiffer than the top layer. When the pile possesses low strength (small values of α_p), the DCM pile fails due to pile head failure as depicted in Fig. 14a. When the conventional DCM pile is transformed to a TDM pile under controlled volume at small α_s (i.e., 1.221), the failure pattern of the TDM pile is the same as that of the DCM pile. However, the zone of MCPs between the surrounding soil and TDM pile extends to a deeper level than for the DCM pile, as shown in Fig. 14b. This difference implies that the load can be transferred to greater depth, and thus larger Q_{ult} can be obtained. When α_s is 1.418 (larger pile cap), a higher load can be transferred to a deeper level. In addition to the MCPs at the pile head and between the surrounding soil and pile, the concentration of MCPs at the pile body immediately beneath the cap can be observed, as illustrated in Fig. 14c. As α_s increases to 2.051 as shown in Fig. 14d, MCPs occur only in the pile body immediately beneath the cap and in the soil surrounding the cap, indicating that failure is dominated by pile body failure. In this case, Q_{ult} is lower than the case with α_s of 1.481 because the part of the abruptly smaller cross section from the cap to the pile body is located at insufficient depth. As a result, the stress suddenly increases at the connection between the cap and the pile body. These results again confirm that a proper design of the shape of the TDM pile is necessary. As α_s increases further to 4.029 and 6.425, as illustrated in Fig. 14e and f, respectively, larger Q_{ult} can be obtained. In both cases, failure is governed by pile body failure.

The failure patterns of the DCM and TDM piles represented by the occurrence of MCPs for piles with q_u of 595 kPa (α_p = 0.85) and various shapes (α_s values) are illustrated in Fig. 15. For the case of α_s = 1.00 (DCM pile), the MCPs were concentrated mainly at the top part of the pile and in the soil surrounding the top part of pile (see Fig. 15a). A pile head failure mode was observed. By comparison with Fig. 14a, the MCPs in the soil surrounding the pile in this case extend to greater depth. When α_s is increased to 1.221, the MCPs are not found within the pile but occur in soil surrounding along the pile shaft and below the pile tip (see Fig. 15b). The failure mode of this case is soil failure. Note that the Q_{ult} is nearly identical to that of the case with α_s = 1.00. Similar results are observed for the cases of α_s = 1.418 and 2.051 (see Fig. 15c and d). However, a few MCPs can also be observed at the pile body just beneath the cap. As α_s increases to 2.865, the MCPs mainly occur in the pile body immediately beneath the cap together and partly in the surrounding soil (see Fig. 15d), exhibiting a pile body-soil failure pattern. For α_s values up to 4.029 and 6.425 (see Fig. 15f–g), similar development of MCPs and failure patterns can be observed. However, the MCPs in the surrounding soil and the pile tip decrease or even vanish.

Fig. 16 shows the failure patterns of piles with high strength (α_p = 1.00) and various values of α_s. Since the pile strength in this case is the optimum value, the DCM pile fails by pile head failure together with soil failure as shown in Fig. 16a. When α_s increases to 1.221 (becoming a TDM pile), as shown in Fig. 16b, soil failure continues to occur. However, Q_{ult} becomes smaller than that of the DCM pile. This decrease is probably due to the decrease in the shaft and tip area of the lower part of pile, which are situated in stiffer and stronger soil. The larger upper part (enlarged cap) is too small to sufficiently absorb the applied

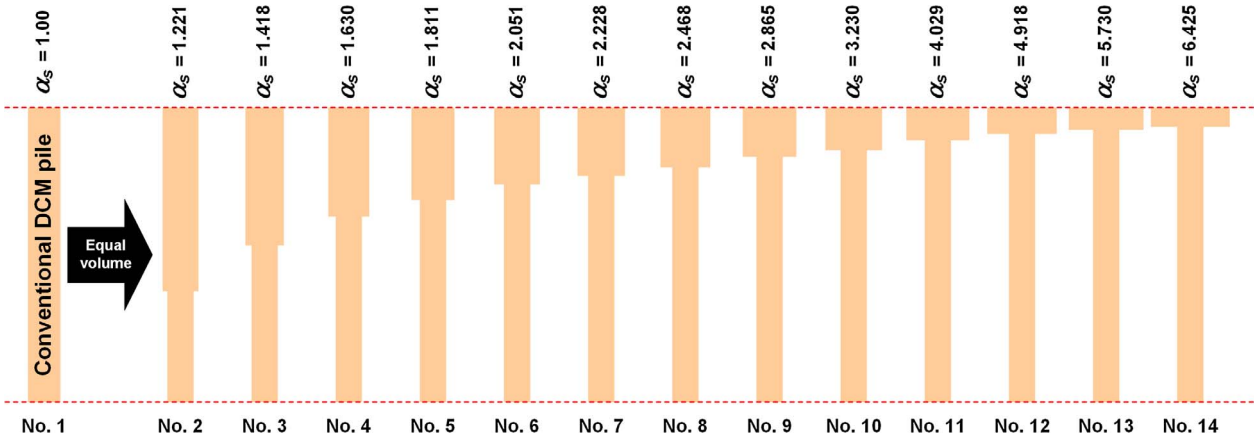

Fig. 13. Schematic of soil-cement piles with varying α_s in the sensitivity analysis.

Table 2
Case investigated in the sensitivity study.

No.	Surface pile diameter (m) D_{DCM} or D_{TDM}	Thick of enlarged pile cap (m) H	Pile body Diameter (m) d_{TDM}	Length of pile (m) L_{DCM} or L_{TDM}	Shape improvement ratio (–) α_s	Pile volume (m^3)	Unconfined compressive strength (kPa) q_u	Strength improvement ratio (–) α_p
1[a]	0.618	–	–	5.600	1.000	1.682	320, 427, 525, 560, 595, 630, 700	0.45, 0.61, 0.75, 0.80, 0.85, 0.90, 1.00
2	0.680	3.490	0.500	5.600	1.221	1.682		
3	0.730	2.620	0.500	5.600	1.418	1.682		
4	0.780	2.070	0.500	5.600	1.630	1.682		
5	0.820	1.760	0.500	5.600	1.811	1.682		
6	0.870	1.460	0.500	5.600	2.051	1.682		
7	0.905	1.300	0.500	5.600	2.228	1.682		
8	0.950	1.140	0.500	5.600	2.468	1.682		
9	1.020	0.940	0.500	5.600	2.865	1.682		
10	1.080	0.810	0.500	5.600	3.230	1.682		
11	1.200	0.620	0.500	5.600	4.029	1.682		
12	1.320	0.500	0.500	5.600	4.918	1.682		
13	1.420	0.420	0.500	5.600	5.730	1.682		
14	1.500	0.370	0.500	5.600	6.425	1.682		

[a] Baseline case (conventional DCM pile, q_u = 700 kPa).

force before transfer to greater depths. This behavior type (soil failure pattern and Q_{ult} less than that of the DCM pile) can be observed with increasing α_s up to 2.051. This pattern indicates that inferior performance would be obtained from transforming a DCM pile to a TDM pile with a size in this range. With greater α_s (4.029 and 6.425), the failure pattern continues to be governed by soil failure, but Q_{ult} becomes larger than that of the DCM pile.

Based on these observations, it was concluded that DCM and TDM piles under the same pile volume can fail in three possible failure patterns, including pile head failure, pile body failure and soil failure. These patterns depend not only on α_s but also on pile strength. The change in the failure pattern (from one TDM shape to another) also affects the change in pile capacity.

(2) Effects of the shape factor (α_s) and strength ratio (α_p) on the ultimate bearing capacity (Q_{ult})

The influence of α_s and α_p on the Q_{ult} of TDM piles is discussed in terms of the ultimate bearing capacity intensity ratio (α_Q), which is defined as

$$\alpha_Q = \frac{Q_{ult} \text{ of conventional DCM or TDM piles}}{Q_{ult} \text{ of baseline case}} \quad (3)$$

Fig. 17 shows the relationship between α_s and α_Q for the various analyzed cases of α_p. The seven symbols in the figure represent seven different failure patterns of the piles as shown in the upper subfigure. Seven lines supersede the seven different α_p of the soil-cement pile, including 0.45, 0.61, 0.75, 0.80, 0.85, 0.90 and 1.00. Each line represents the computed results from cases with various dimension following Fig. 13. For the data set with α_p of 0.45 and 0.61, α_Q increases considerably (from α_s = 1.00 for the conventional DCM pile with a pile head failure pattern) with increasing α_s until reaching values of 1.630 and 1.418, respectively. At these points (star symbol), the top part of the enlarged pile cap and the pile body immediately below the enlarged pile cap fail simultaneously (pile head-body failure pattern). When α_s increases (larger cap dimension), α_Q gradually decreases until α_s reaches 2.468. Beyond that, α_Q continues to increase again, and the failure pattern is governed by pile body failure. Moreover, based on the results for α_p = 0.45, after the reduction of α_Q in the range of 1.630–2.468, α_Q returns to the previous peak value (0.788 at α_s of 1.630) when α_s is equal to 4.3. The failure pattern changes from pile head-body failure to pile body failure. This phenomenon is similar to the results for the case with α_p = 0.61; after decreasing, α_Q increases and approaches the previous peak value at α_s of 4.45. However, for these two pile strengths, α_Q is larger for all TDM pile shapes (all α_s values) than that of the DCM pile of the same strength, indicating the advantage of transforming a DCM pile to a TDM pile. Moreover, for the largest cap considered in this study (α_s of 6.425), the TDM pile with low strength (α_p of 0.61) offers the same pile capacity as the DCM in the baseline case (higher strength).

For the data set with α_p of 0.75 and 0.80, the failure pattern changes from pile head failure (for α_s = 1.00) to soil failure with α_s increasing in the range of 1.221–2.468 with a slight increase in α_Q. When α_s exceeds 2.468, the failure is dominated by pile body failure with gradually

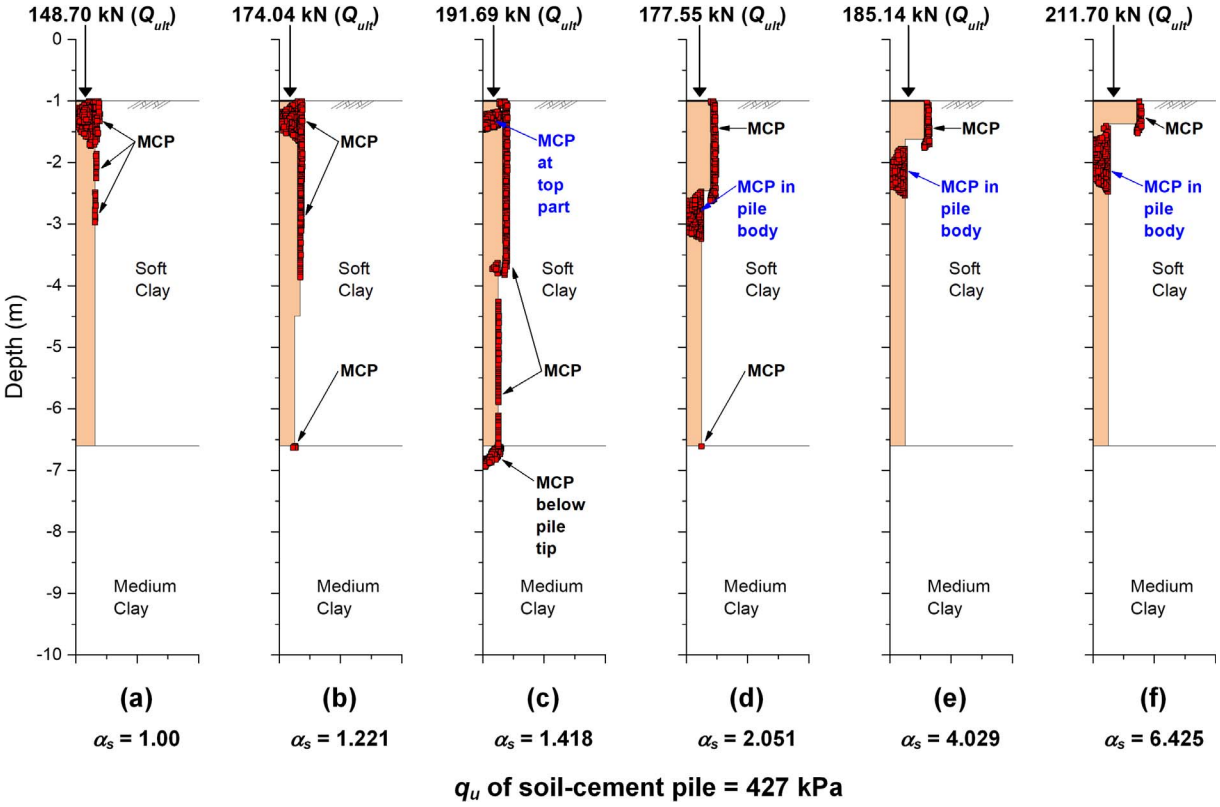

Fig. 14. Mohr-Coulomb points of conventional DCM and TDM piles having q_u of 427 kPa (α_p = 0.61) at failure load with constant pile volume and varying α_s.

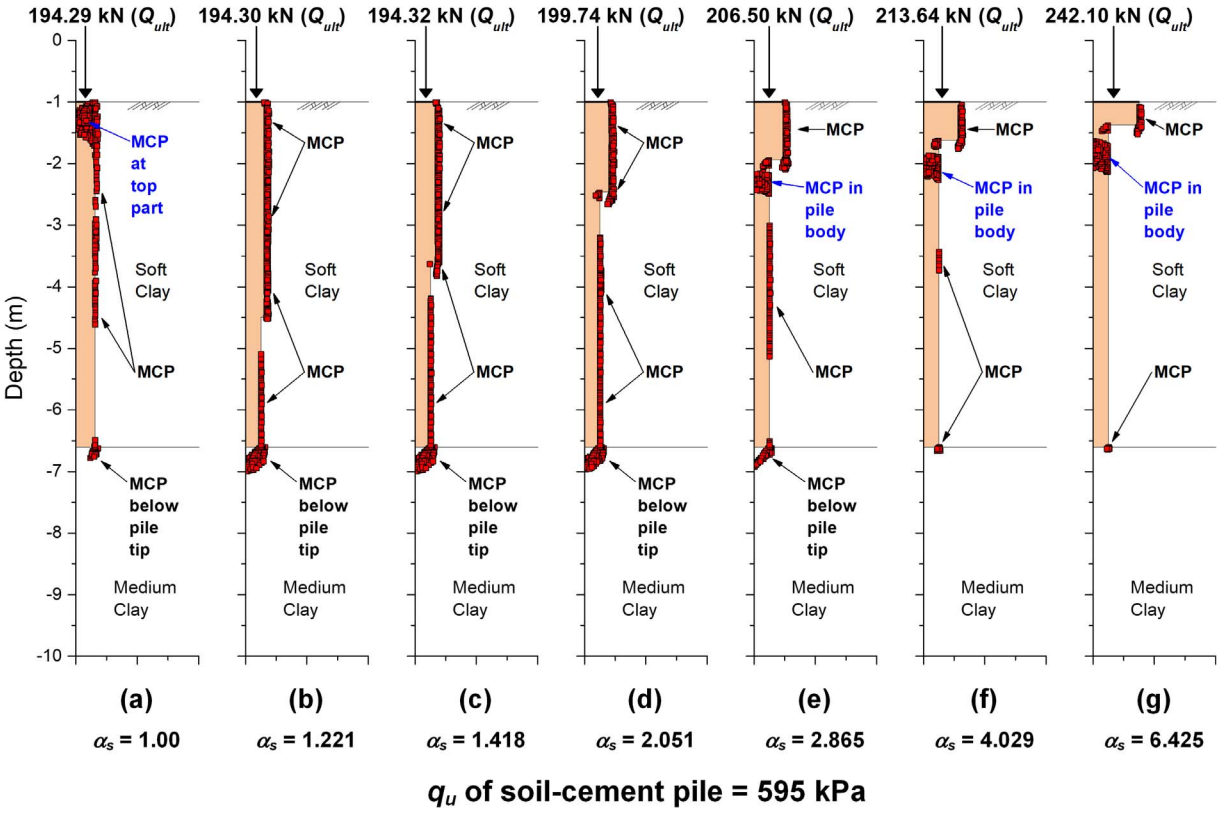

Fig. 15. Mohr-Coulomb points of conventional DCM and TDM piles having q_u of 595 kPa (α_p = 0.85) at failure load with constant pile volume and varying α_s.

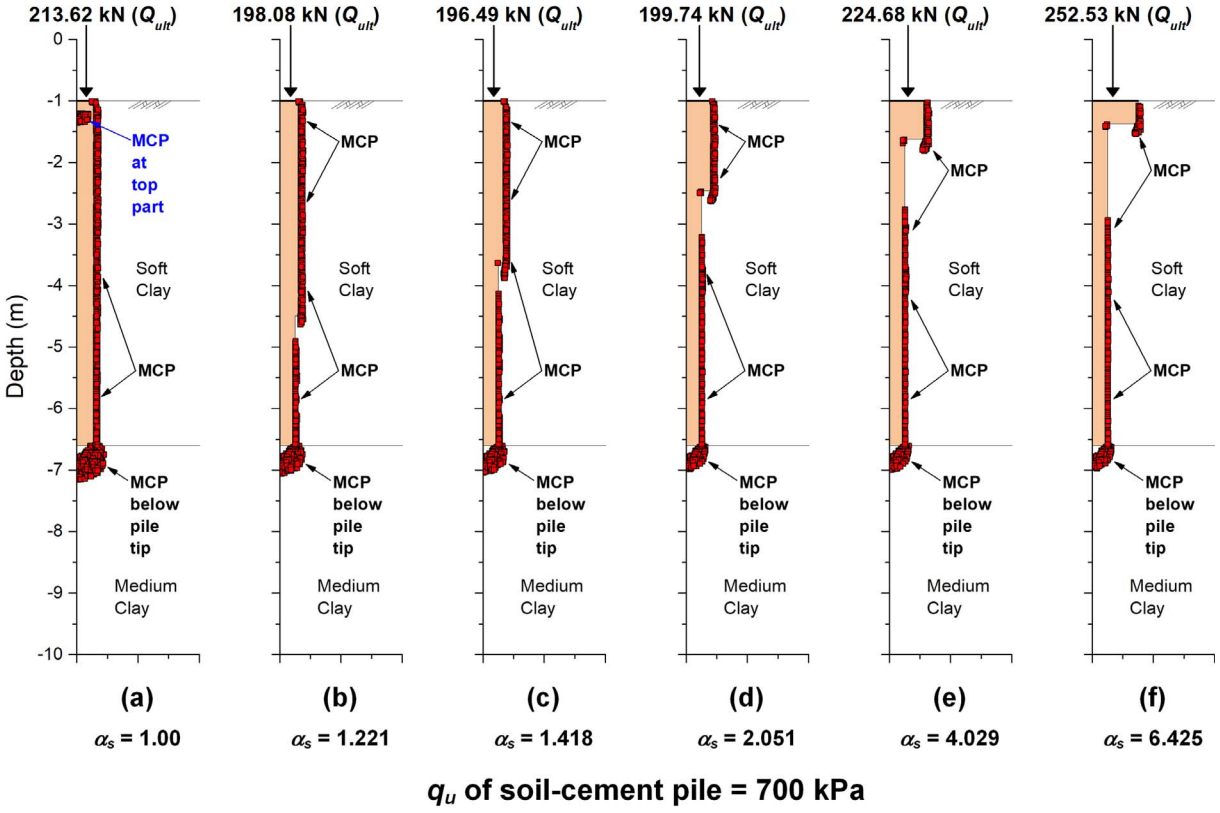

Fig. 16. Mohr-Coulomb points of conventional DCM and TDM piles having q_u of 700 kPa (α_p = 1.00) at failure load with constant pile volume and varying α_s.

increasing α_Q. For all TDM pile shapes with this range of α_p, α_Q is also larger than that of the conventional DCM pile with the same strength. For piles with α_p of 0.85, α_Q continues increasing with increasing α_s. The failure pattern consequently changes from pile head failure (for the DCM pile) to soil failure, pile body-soil failure and pile body failure with increasing α_s.

At higher values of α_p (0.90 and 1.00), α_Q decreases when the DCM pile is transformed to a TDM pile with the α_s in the range of 1.00 to 2.865. The pile head failure of the DCM pile also changes to soil failure for the TDM piles. Thus, transforming a DCM pile to a TDM pile does not always guarantee superior performance. When α_s increases beyond 3.0, the benefit of transforming a DCM pile to a TDM pile is evident. The soil failure mode is maintained with an enlarged pile cap for this case.

From the above-described results, it is concluded that both cap shape and pile strength play important roles in both the TDM pile capacity and the failure pattern. Under constant volume, transforming the DCM pile to a TDM pile does not guarantee superior performance unless both factors are taken into consideration. To ensure that the transformation to a TDM pile will be effective regardless of pile strength, the shape corresponding to an α_s of greater than 3.0 is recommended. For a small enlarged pile cap (α_s less than 3.0), pile strength corresponding to a maximum α_Q of 0.85 is suggested. It is also possible to achieve pile capacity equivalent to the DCM pile at optimal strength by transformation to a TDM pile with lower strength. This finding is very interesting for the use of TDM piles to reduce construction costs.

(3) Mobilization of side and tip resistances at the ultimate bearing capacity (Q_{ult})

The load sharing between the side and tip resistances of the piles at Q_{ult} is further investigated to obtain a better understanding of how Q_{ult} and probably the failure pattern change with the shape factor (α_s). Under a given applied load, the pile-supported load is carried partly by the side resistance at the perimeter surface of the enlarged pile cap and pile body (Q_{sc} and Q_{sp}) and partly by the tip resistance below the enlarged pile cap (Q_{bc}) and below the pile body (Q_{bp}). Fig. 18 presents the mobilized side and tip resistances of the conventional DCM and TDM piles with various shapes with α_p of 0.61 (representing low-strength piles). For the DCM pile (α_s = 1.00), the entire load-carrying ability comes from the side resistance between the pile and the surrounding soil. This is due to the low strength of the pile. Failure occurs at the pile head before the load is transferred to the pile tip. By transforming to a TDM pile (α_s larger than 1.00), the load is shared by all four components. Thus, the applied load can be transferred to the tip, resulting in an increase in Q_{ult}. For the TDM pile with α_s of 1.221 and a thick but small cap, the major contribution is the side resistance of the cap (Q_{sc}). With increasing α_s or a larger but thinner cap, the contribution from Q_{sc} decreases with compensation by cap bearing (Q_{bc}). However, the contribution from the cap (Q_{sc} + Q_{bc}) increases. For TDM piles with α_s of 1.418, which offers the peak Q_{ult}, failure occurs at both the head and pile body simultaneously, and Q_{sp} drastically increases.

For TDM piles with α_s greater than 1.630, in which failure is governed by pile body failure, the increase in Q_{ult} comes directly from the contribution from the cap. Q_{sp} is virtually constant at approximately 80 kN for α_s greater than 2.051. This corresponds to the available maximum compressive load of the pile body ($q_u \times A_{d,TDM}$ = 427 × π·0.5^2/4 = 83.84 kN). The benefit of enlarging the pile cap is thus due to the drastic increase in Q_{bc} compared to the decrease in Q_{sc}. The performance of the low-strength TDM piles is limited by the ability to sustain the load at the pile body.

Fig. 19 shows the mobilized resistances of DCM and TDM piles of various shapes and α_p of 1.00 (refer to the high-strength pile). As shown in the figure, for α_s = 1.00 (conventional DCM pile), the pile fails by pile head failure together with soil failure. Q_{ult} is contributed by the ultimate side and tip resistances. For the cases of α_s > 1.00 (TDM piles), Q_{bp} becomes smaller than that of the DCM pile due to the smaller pile body, resulting in smaller Q_{ult} when the DCM pile is transformed to a TDM pile

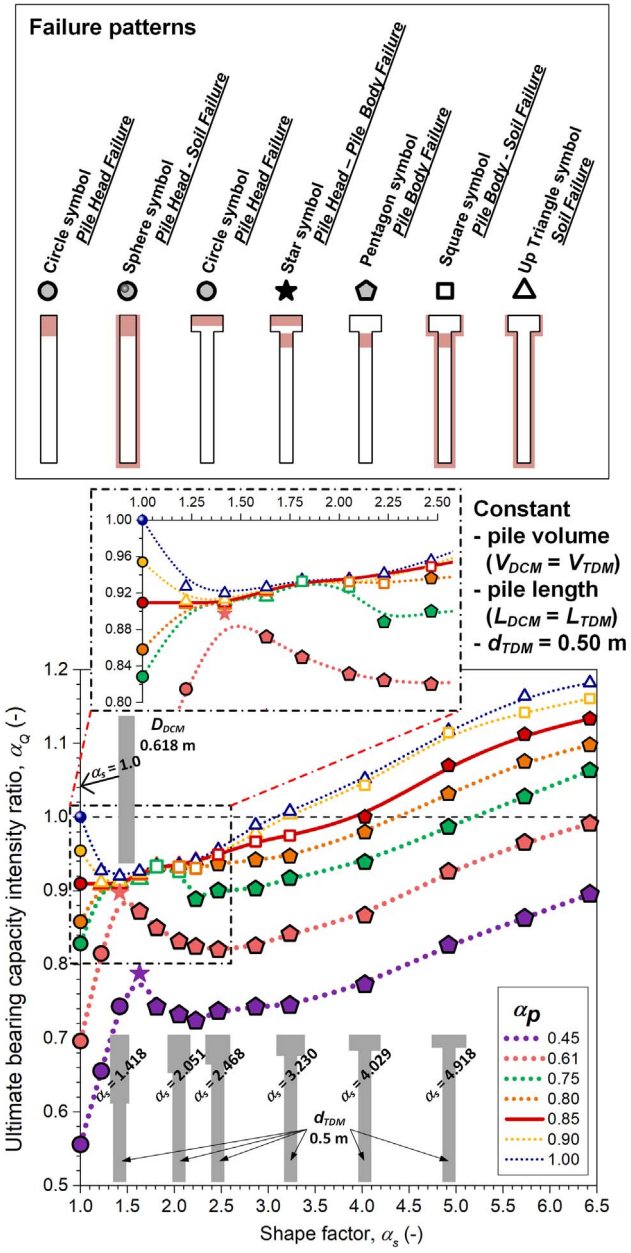

Fig. 17. α_s versus ultimate bearing capacity intensity of piles with various strengths and associated failure patterns.

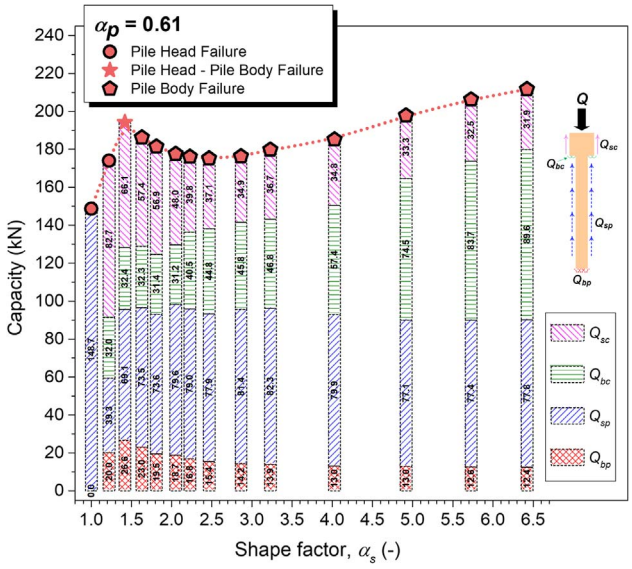

Fig. 18. Mobilized shaft and tip resistances of piles with various shapes at α_p of 0.61.

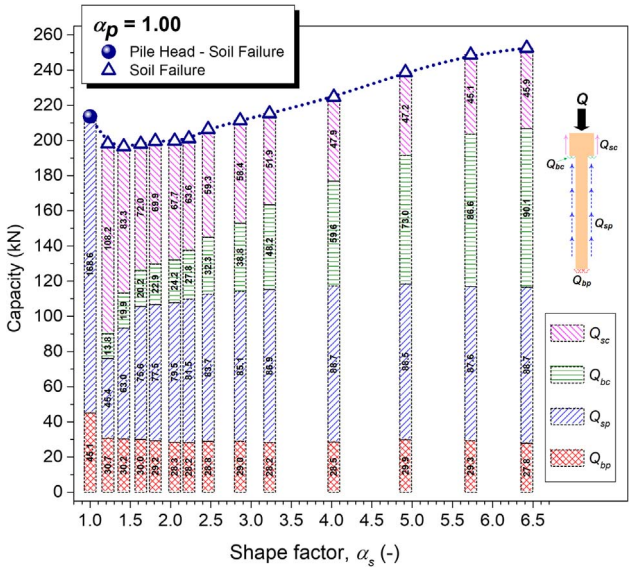

Fig. 19. Mobilized shaft and tip resistances of piles with various shapes at α_p of 1.00.

with a small cap dimension. Q_{bp} remains practically unchanged at 30.0 kN with increasing α_s, implying that this value is the ultimate value the soil at the tip can offer for this size of pile body. By contrast, Q_{sp} continually increases as the length of the pile body increases. Based on back calculation, it can be determined that Q_{sp} is the available maximum pile body skin friction provided by the surrounding soil. It is also observed in the figure that Q_{ult} of the TDM pile is principally affected by Q_{sc} and Q_{bc}.

6. Conclusion

A series of 2D-FE simulations of pile load tests on DCM and TDM piles extended from a reference case were conducted to investigate their load carrying and failure behaviors under controlled pile volume and length. The main focus was effect of the interaction between the shape of the enlarged pile cap and pile strength on those behaviors. A parameter, the shape factor (α_s), is introduced to represent the shape and size of the pile cap. Scaled-down model tests on conventional DCM and TDM piles in the laboratory verified the findings from the preliminary simulation. Additional sensitivity analyses further clarified the effects of the complex interaction of the shape of the enlarged pile cap and pile strength on the pile behaviors. The results are as follows:

(1) Under the same pile volume, enlarging the pile cap does not guarantee an increase in pile ultimate capacity. In addition, the pile strength in relation to the optimum DCM pile strength (α_p) plays an important role in the change in pile capacity.
(2) For relatively high pile strength (α_p > 0.85), enlarging the pile cap by a small degree (α_s < 1.75) leads to a decrease in the pile ultimate capacity followed by an increasing trend. By contrast, a rapid increase in the pile ultimate capacity is obtained when the pile cap is enlarged to a small degree at medium-high pile strength (α_p < 0.85). Beyond an α_s of 1.75, the pile ultimate capacity decreases in a narrow range (1.75 < α_s < 2.50) before continuously increasing.
(3) To guarantee the effectiveness of enlarging the pile cap, an α_s of not less than 3.00 is recommended.
(4) The effects of cap shape and pile strength on the failure pattern and

bearing capacity of TDM piles are attributed to changes in load transfer mechanism, which in turn depend on the mobilized skin friction and bearing by both the cap and the pile body.

(5) By enlarging the pile cap with an appropriate shape factor, the pile strength can be decreased to achieve the same or even greater ultimate pile capacity.

Acknowledgments

The authors would like to express their gratitude for financial support from King Mongkut's University of Technology Thonburi (KMUTT) and the Thailand Research Fund (TRF) through The Petchra Pra Jom Klao PhD scholarship under contract Grant No. 32/2558 and TRF Basic Research Grant No. BRG6080011. The support from the Faculty of Engineering, King Mongkut's University of Technology North Bangkok (KMUTNB) under contract No. ENG-60-20 is also acknowledged.

References

[1] Bergado DT, Ruenkrairergsa T, Taesiri Y, Balasubramaniam AS. Deep soil mixing used to reduce embankment settlement. Gr Improv 1999;3:145–62. http://dx.doi.org/10.1680/grim.1999.3.4.145.

[2] Chai JC, Shrestha S, Hino T, Ding WQ, Kamo Y, Carter J. 2D and 3D analyses of an embankment on clay improved by soil-cement columns. Comput Geotech 2015;68:28–37. http://dx.doi.org/10.1016/j.compgeo.2015.03.014.

[3] Jamsawang P, Yoobanpot N, Thanasisathit N, Voottipruex P, Jongpradist P. Three-dimensional numerical analysis of a DCM column-supported highway embankment. Comput Geotech 2016;72:42–56. http://dx.doi.org/10.1016/j.compgeo.2015.11.006.

[4] Lai YP, Bergado DT, Lorenzo GA, Duangchan T. Full-scale reinforced embankment on deep jet mixing improved ground. Gr Improv 2006;10:153–64. http://dx.doi.org/10.1680/grim.2006.10.4.153.

[5] Venda Oliveira PJ, Pinheiro JLP, Correia AAS. Numerical analysis of an embankment built on soft soil reinforced with deep mixing columns: parametric study. Comput Geotech 2011;38:566–76. http://dx.doi.org/10.1016/j.compgeo.2011.03.005.

[6] Venda Oliveira PJ, Correia AAS, Lemos LJL. Numerical prediction of the creep behaviour of an unstabilised and a chemically stabilised soft soil. Comput Geotech 2017;87:20–31. http://dx.doi.org/10.1016/j.compgeo.2017.02.006.

[7] Voottipruex P, Suksawat T, Bergado DT, Jamsawang P. Numerical simulations and parametric study of SDCM and DCM piles under full scale axial and lateral loads. Comput Geotech 2011;38:318–29. http://dx.doi.org/10.1016/j.compgeo.2010.11.006.

[8] Voottipruex P, Bergado DT, Suksawat T, Jamsawang P, Cheang W. Behavior and simulation of deep cement mixing (DCM) and Stiffened Deep Cement Mixing (SDCM) Piles Under Full Scale Loading. Soils Found 2011;51:307–20. http://dx.doi.org/10.3208/sandf.51.307.

[9] Yapage NNS, Liyanapathirana DS, Kelly RB, Poulos HG, Leo CJ. Numerical modeling of an embankment over soft ground improved with deep cement mixed columns: case history. J Geotech Geoenviron Eng 2014;140:4014062. http://dx.doi.org/10.1061/(ASCE)GT.1943-5606.0001165.

[10] Jamsawang P, Voottipruex P, Boathong P, Mairaing W, Horpibulsuk S. Three-dimensional numerical investigation on lateral movement and factor of safety of slopes stabilized with deep cement mixing column rows. Eng Geol 2015;188:159–67. http://dx.doi.org/10.1016/j.enggeo.2015.01.017.

[11] Jamsawang P, Boathong P, Mairaing W, Jongpradist P. Undrained creep failure of a drainage canal slope stabilized with deep cement mixing columns. Landslides 2016;13:939–55. http://dx.doi.org/10.1007/s10346-015-0651-9.

[12] Larsson S, Malm R, Charbit B, Ansell A. Finite element modelling of laterally loaded lime-cement columns using a damage plasticity model. Comput Geotech 2012;44:48–57. http://dx.doi.org/10.1016/j.compgeo.2012.03.004.

[13] Ignat R, Baker S, Larsson S, Liedberg S. Two- and three-dimensional analyses of excavation support with rows of dry deep mixing columns. Comput Geotech 2015;66:16–30. http://dx.doi.org/10.1016/j.compgeo.2015.01.011.

[14] Jamsawang P, Jamnam S, Jongpradist P, Tanseng P, Horpibulsuk S. Numerical analysis of lateral movements and strut forces in deep cement mixing walls with top-down construction in soft clay. Comput Geotech 2017;88:174–81. http://dx.doi.org/10.1016/j.compgeo.2017.03.018.

[15] CDIT (Coastal Development Institute of Technology). The Deep Mixing Method: Principle, Design and Construction. A.A. Balkema, The Netherlands; 2002.

[16] Petchgate K, Jongpradist P, Panmanajareonphol S. Field pile load test of soil-cement column in soft clay. Proc Int Symp 2003 Soil/gr Improv Geosynth Waste Contain Eros Control Appl 2003;2003:175–84.

[17] Uddin K, Balasubramaniam AS, Bergado DT. Engineering behavior of cement-treated Bangkok soft clay. Geotech Eng 1997;28:89–119.

[18] Lorenzo GA, Bergado DT, Soralump S. New and economical mixing method of cement- admixed clay for DMM Application. Geotech Test J 2006;29:54–63. http://dx.doi.org/10.1520/GTJ12129.

[19] Jongpradist P, Youwai S, Jaturapitakkul C. Effective void ratio for assessing the mechanical properties of cement-clay admixtures at high water content. J Geotech Geoenviron Eng 2011;137:621–7. http://dx.doi.org/10.1061/(ASCE)GT.1943-5606.0000462.

[20] Chen L, Liu SY. Consolidation calculation of soft ground improved by T-shape deep mixing columns. GeoCongress 2008 Geosustainability Geohazard Mitigation, March 9, 2008 - March 12, 2008; 2008. p. 620–7. http://dx.doi.org/10.1061/40971(310)77.

[21] Yi YL, Liu SY. Bearing behavior of single T-shaped cement-soil deep mixing column. Proc Int Symp Lowl Technol 2008:261–5.

[22] Wonglert A, Jongpradist P. Impact of reinforced core on performance and failure behavior of stiffened deep cement mixing piles. Comput Geotech 2015;69:93–104. http://dx.doi.org/10.1016/j.compgeo.2015.05.003.

[23] Liu SY, Du YJ, Yi YL, Puppala AJ. Field investigations on performance of T-shaped deep mixed soil cement column-supported embankments over soft ground. J Geotech Geoenviron Eng 2012;138:718–27. http://dx.doi.org/10.1061/(ASCE)GT.1943-5606.0000625.

[24] Yi YL, Liu SY, Puppala AJ, Xi PS. Vertical bearing capacity behaviour of single T-shaped soil–cement column in soft ground: laboratory modelling, field test, and calculation. Acta Geotech 2017:1–12. http://dx.doi.org/10.1007/s11440-017-0555-z.

[25] Yi YL, Liu SY, Puppala AJ. Laboratory modelling of T-shaped soil–cement column for soft ground treatment under embankment. Géotechnique 2016;66:85–9. http://dx.doi.org/10.1680/jgeot.15.P.019.

[26] Jamsawang P, Bergado DT, Voottipruex P. Field behaviour of stiffened deep cement mixing piles. Proc Inst Civ Eng - Gr Improv 2011;164:33–49. http://dx.doi.org/10.1680/grim.900027.

[27] De Beer EE. Proefondervindlijke bijdrage tot de studie van het grensdraag vermogen van zand onder funderingen op staal. Tijdshift Der Openbar Verken van Belgie; 1967.

[28] Schanz T, Vermeer A, Bonnier P. The hardening soil model: formulation and verification. Beyond 2000 Comput Geotech 10 Years PLAXIS. In: Int proc int symp beyond 2000 comput geotech Amsterdam Netherlands 1820 March 1999; 1999, 281.

[29] Rukdeechuai T, Jongpradist P, Wonglert A, Kaewsri T. Influence of soil models on numerical simulation of geotechnical works in Bangkok subsoil. EIT Res Dev J 2009;20:17–28.

[30] Prust RE, Davies J, Hu S. Part 6: tunnels and underground structures: pressuremeter investigation for mass rapid transit in Bangkok, Thailand. Transp Res Rec J Transp Res Board 2005;1928:207–17. http://dx.doi.org/10.3141/1928-22.

[31] Jongpradist P, Kaewsri T, Sawatparnich A, Suwansawat S, Youwai S, Kongkitkul W, et al. Development of tunneling influence zones for adjacent pile foundations by numerical analyses. Tunn Undergr Sp Technol 2013;34:96–109. http://dx.doi.org/10.1016/j.tust.2012.11.005.

[32] Lueprasert P, Jongpradist P, Jongpradist P, Suwansawat S. Numerical investigation of tunnel deformation due to adjacent loaded pile and pile-soil-tunnel interaction. Tunn Undergr Sp Technol 2017;70:166–81. http://dx.doi.org/10.1016/j.tust.2017.08.006.

[33] Jamsawang P, Voottipruex P, Jongpradist P, Bergado DT. Parameters affecting the lateral movements of compound deep cement mixing walls by numerical simulations and parametric analyses. Acta Geotech 2015;10:797–812. http://dx.doi.org/10.1007/s11440-015-0417-5.

[34] Jongpradist P, Jumlongrach N, Youwai S, Chucheepsakul S. Influence of fly ash on unconfined compressive strength of cement-admixed clay at high water content. J Mater Civ Eng 2010;22:49–58. http://dx.doi.org/10.1061/(ASCE)0899-1561(2010) 22:1(49).

[35] Shen SL, Wang ZF, Horpibulsuk S, Kim YH. Jet grouting with a newly developed technology: The Twin-Jet method. Eng Geol 2013;152:87–95. http://dx.doi.org/10.1016/j.enggeo.2012.10.018.